Electronic Supplementary Material (ESI) for Journal of Materials Chemistry A.

Supporting Information

A new carbon-black/cellulose-sponge system with water supplied by injection for enhancing solar vapor generation

Shang Liu, **Congliang Huang***, Qiangqiang Huang, Fengchao Wang, Chuwen Guo

School of Electrical and Power Engineering, China University of Mining and Technology, Xuzhou 221116, China.

*Corresponding Author, E-mail: huang198564@gmail.com

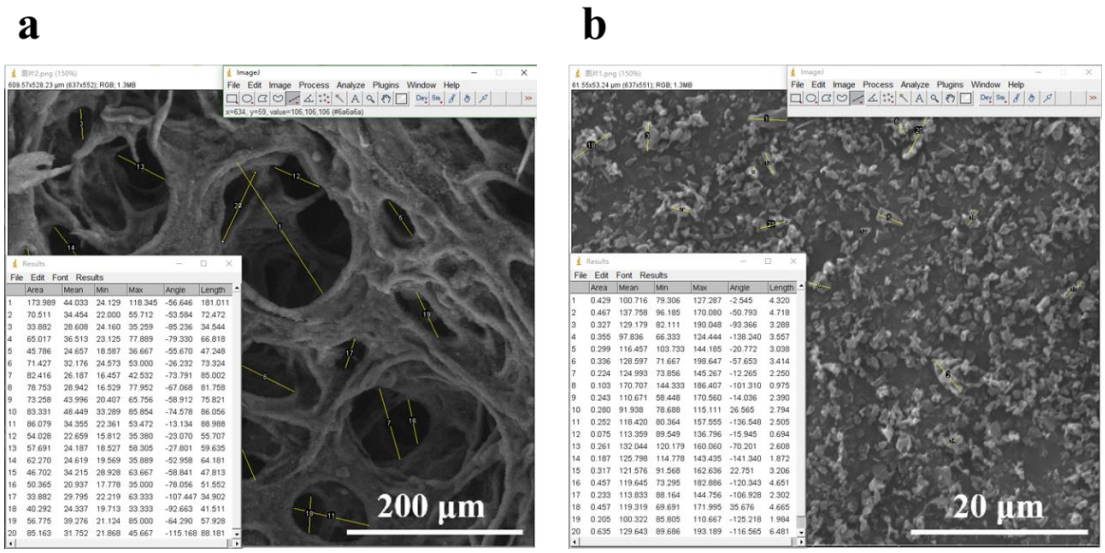

Figure S1. Statistical diagram of (a) pore size in cellulose sponge and (b) carbon black particle size using ImageJ.

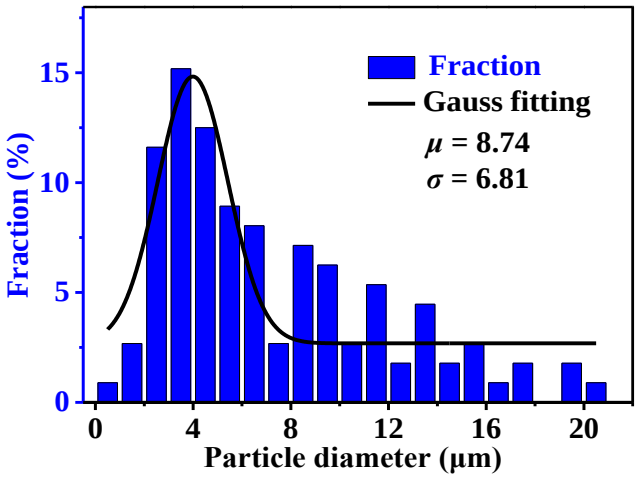

Figure S2. Diameter distributions of carbon black particles.

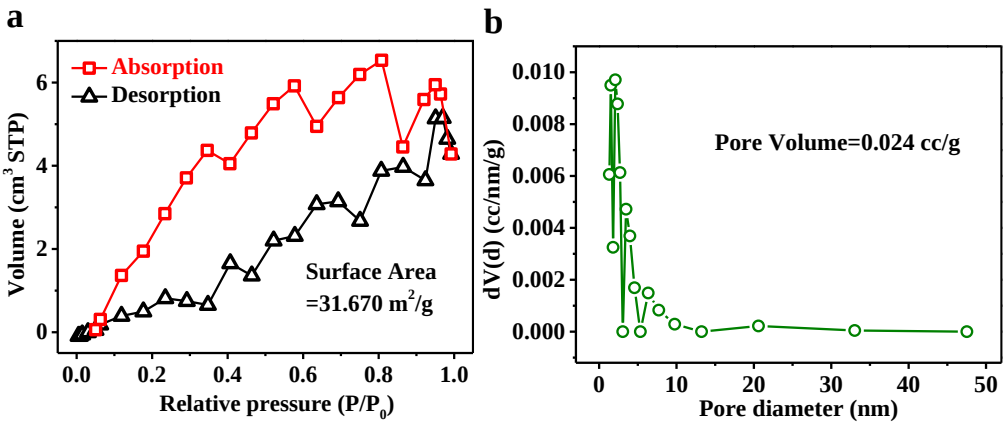

Figure S3. (a) N_2 absorption and desorption isotherm linear plot of CBCS and (b) the corresponding pore size distributions.

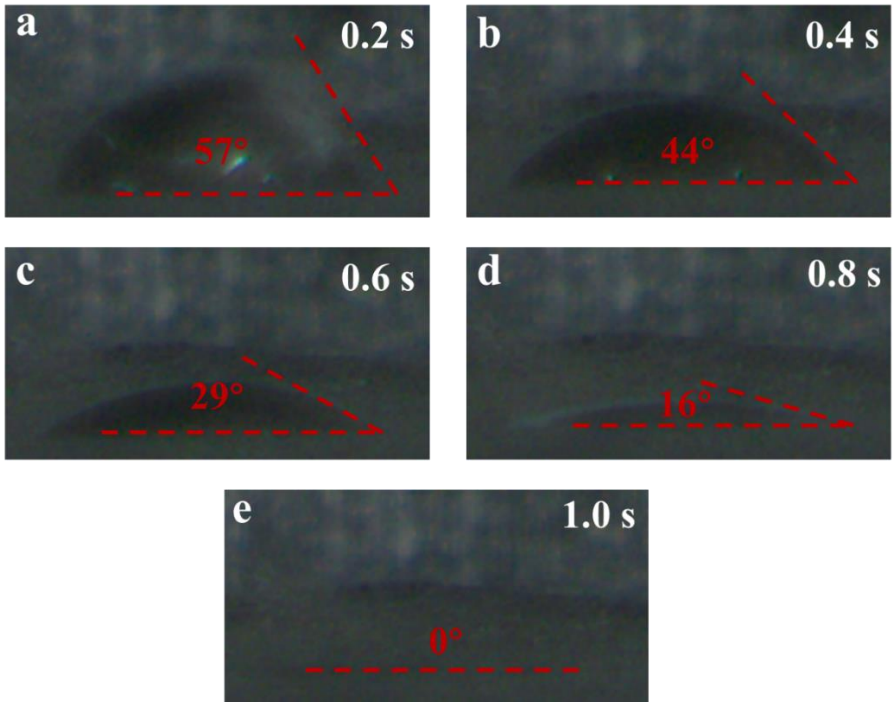

Figure S4. Dynamic contact angle of the CBCS.

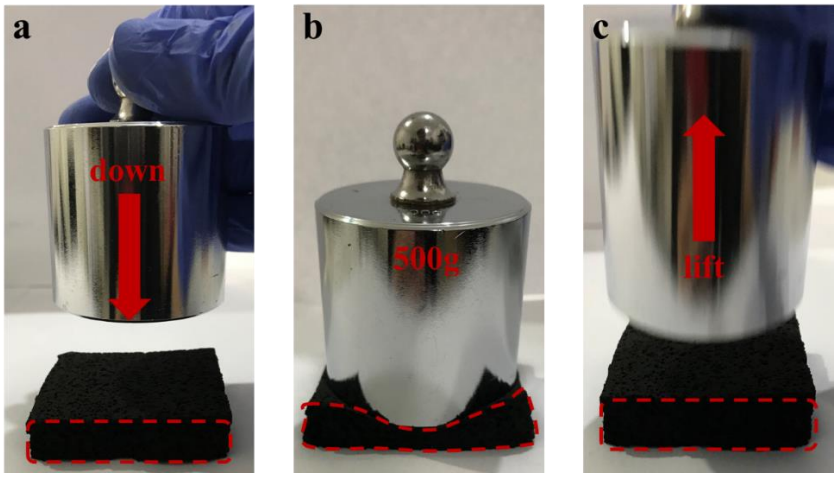

Figure S5. Compression tests of CBCS.

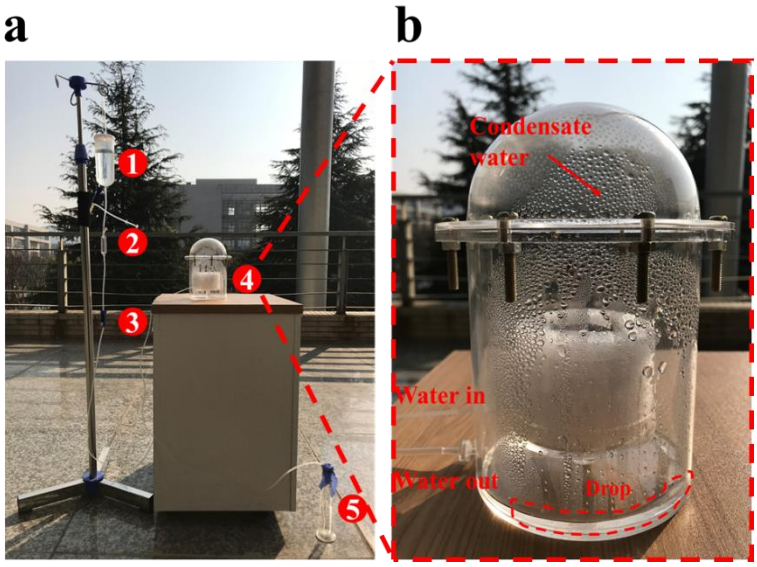

Figure S6. (a) Experimental system: ① seawater storage bottle, ② Murphy's dropper, ③ regulator, ④ evaporation part and ⑤ freshwater collection bottle. (b) Zoom-in image of evaporation part.

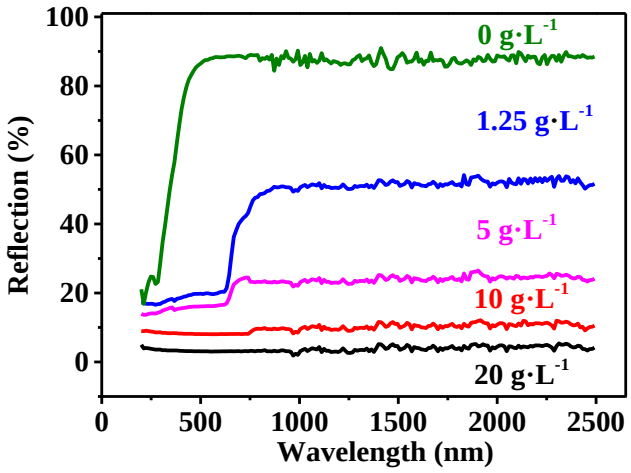

Figure S7. Reflection spectrum of the CBCS at wet state.

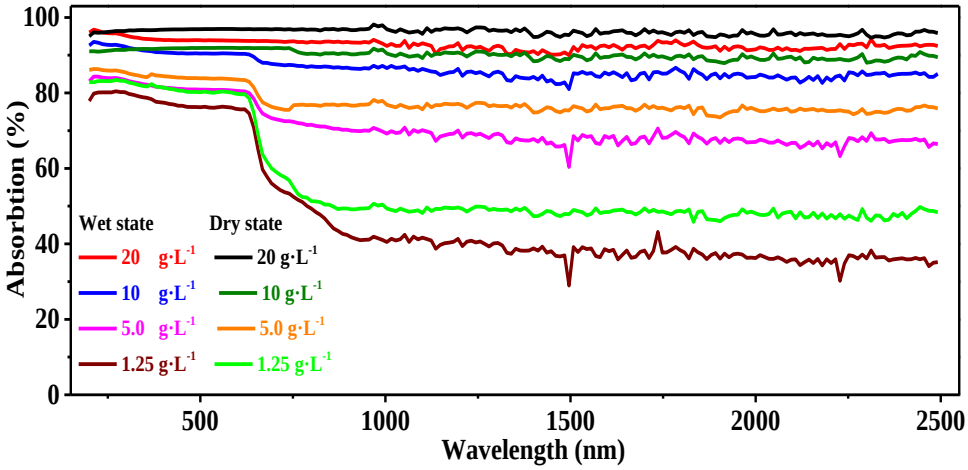

Figure S8. Absorption of the CBCS with different carbon black concentrations in dry and wet state.

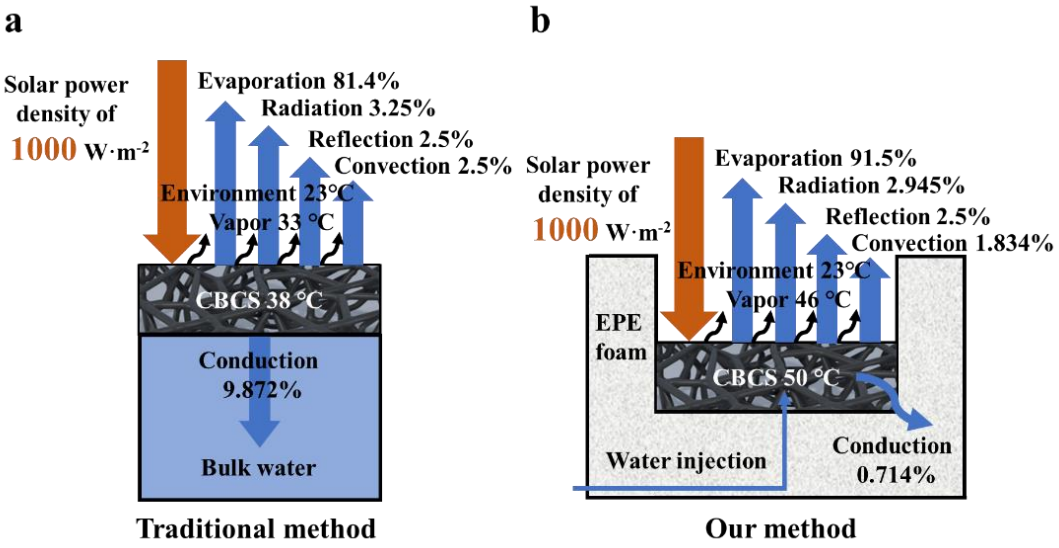

Figure S9. The energy analysis of traditional method (a) and CBCS system (b) under 1000 W·m^{-2} irradiation density.

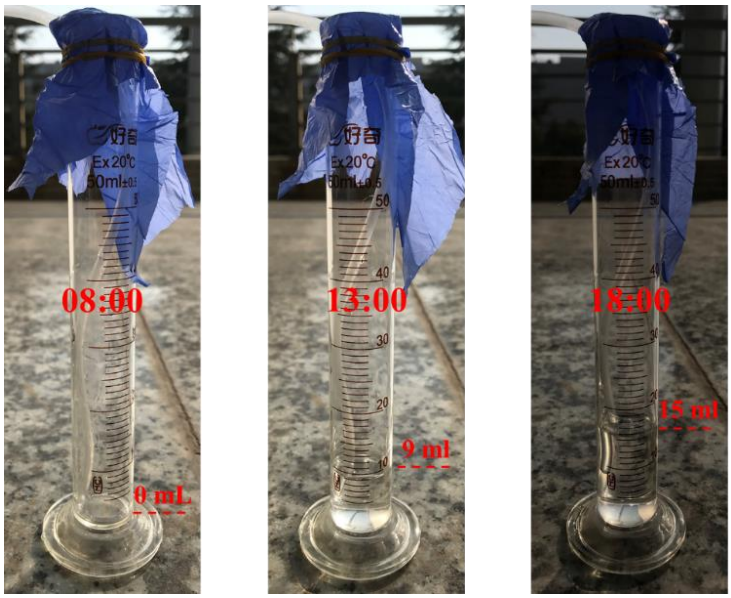

Figure S10. Amount of fresh water collected in graduated cylinder at different times (8:00, 13:00 and 18:00).

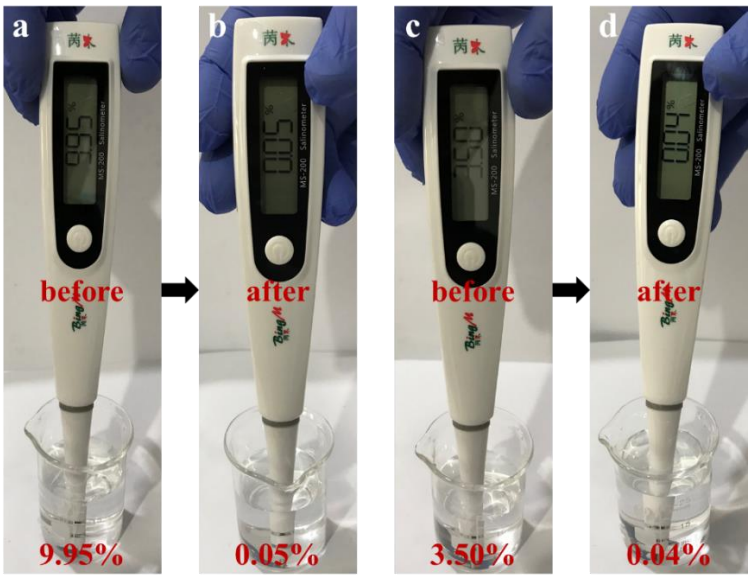

Figure S11. Salinity comparisons between the simulated seawater (3.5 and 10 % NaCl solution) and the fresh water.

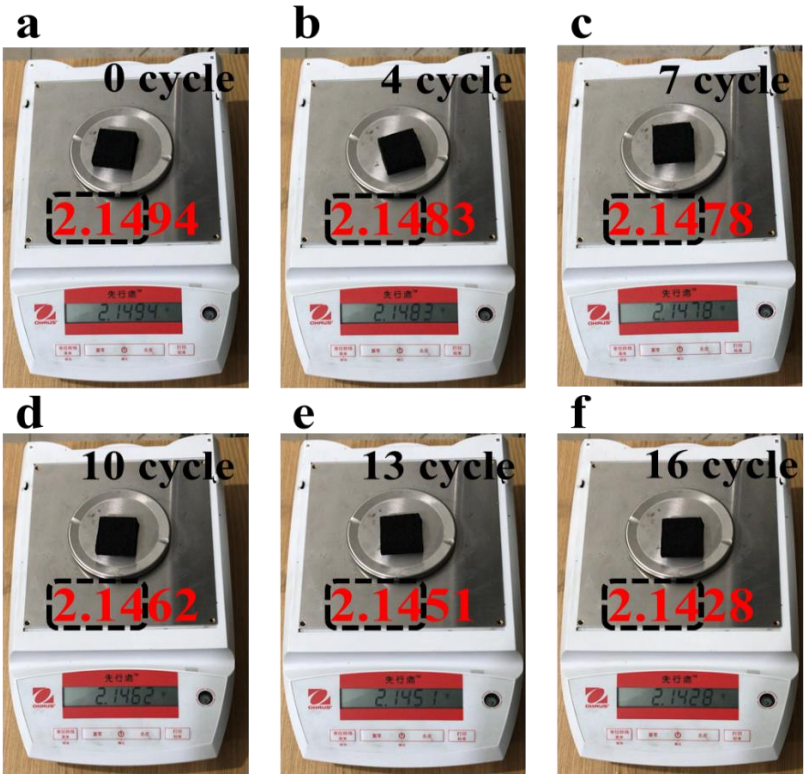

Figure S12. Weight of CBCS after cycles of use.

Table S1. Details about the experimental instruments used in this work.

Function	Equipment	Model	Manufacturer
Preparation	Ultrasonic Cell Crusher	JY92-IIN	Ningbo Xinzhi Biotechnology Co., Ltd.
	Vacuum Drying Oven	DZF-6050	Shanghai Donglu Instrument Equipment Co., Ltd.
Characterization	Thermal Conductivity Instrument	Model TC3000	Xian XIATECH Technology Co., Ltd.
	Automatic Gas Adsorption Analyzer	Autosorb-LQ3	Quantachrome Ins, U.S.A.
	Universal Electronic Testing Machine	UTM4203X	Shenzhen Sansizongheng Technology Co., Ltd.
	High-Speed Camera	1F005	Hefei Fuhuang Junda Hi-Tech Information Technology Co., Ltd.
	Scanning Electron Microscope (SEM)	Quanta 250	FEI, U.S.A.
	Fourier Transform Infrared (FTIR) Spectroscopy	VERTEX 80v	Bruker, Karlsruhe, Germany
	X-ray photoelectron spectroscopy (XPS)	ESCALAB 250Xi	Thermo Fisher, USA
	Ultraviolet-Visible-Near Infrared Spectrophotometer	UV-3600	Shimadzu Enterprise Management (China) Co., Ltd.
	Laser Ablation Inductively Coupled Plasma Mass Spectrometer	NWR 213-7900 ICP-MS	Agilent, China
Process Monitor	Solar Illumination Simulator	BOS-X-350G	Changchun Ocean Photoelectric Co., Ltd.
	Solar Power Meter	SM206	Xinbao Keyi Co., Ltd.
	Data Acquisition Instrument	Keithley 2700	Keithley Instruments Inc. Clevelan, Ohio, U.S.A.

	Electronic Microbalance	OHAUS CP224C	OHAUS Instruments (Changzhou) Co., Ltd.
	IR Camera	FLUKE ti9	Fluke electronic instruments and instruments company

Table S2. Calculation of the total enthalpy of water liquid-vapor phase change at different surface temperatures.

Solar power density ($W \cdot m^{-2}$)	**Sample**	**Concentration of carbon black particles ($g \cdot L^{-1}$)**	**Surface temperature (°C)**	**Δh_{vap} ($kJ \cdot kg^{-1}$)**	**h_{LV} ($kJ \cdot kg^{-1}$)**
1000	CBCS	0	30	2429.7	2454.8
1000	CBCS	1.25	35	2417.8	2463.8
1000	CBCS	5	40	2405.9	2472.8
1000	CBCS	10	45	2393.9	2481.7
1000	CBCS	20	50	2381.9	2490.6
800	CBCS	20	41	2403.5	2470.4
600	CBCS	20	33	2422.6	2460.2
400	CBCS	20	29	2432.1	2457.2
200	CBCS	20	21	2450.9	2442.6

Table S3. Efficiency of different solar vapor generation system under different ambient temperatures.

Materials	**Solar density ($kW \cdot m^2$)**	**Ambient temperature (°C)**	**Surface temperature (°C)**	**Evaporation rate ($kg \cdot m^{-2} \cdot h^{-1}$)**	**Efficiency (%)**	**Ref.**
Graphene oxide-Wood	12	27	70	10.08	82.8	24

Gold nanoparticle-airlaid paper	4.5	27	80		77.8	22
Carbon nanotube-airlaid paper	5			3.615	40	23
Surface-carbonized longitudinal wood	10	20	90	1.08	89	28
Recycled waste black polyurethane sponges	3	21	56.3	2.5	55	45
Carbonized mushrooms	1	21	38	1.475	78	14
Black Titania with Unique Nanocage Structure	1	30	80	1.13	70.9	36
Flame-treated wood	1	31.5	43	1.05	72	44
Commercially Available Activated Carbon Fiber Felt	1	26.3	48	1.22	79.4	16
GO-flim-cellulose with 2D water path	1	12.9	38.8	1.45	80	27
Au NPs-airlaid paper	10	20		11.8	85	19
Graphene Oxide-Polyurethane Nanocomposite Foam	10			11.24	81	18
Graphite powder/semipermeable collodion membrane	3	22	42.4	1.36	65.8	26
Double-layer rGO/MCE systems	1	25	40.5	0.838	60	21
CNT/silica bilayer	1	22		1.29	82	32
F-Wood/CNTs	1	20	36.2	0.95	65	34

Note S1

Reflectivity calculation

As described by the Fresnel equation, the reflectivity between different mediums can be calculated by,

$$R = (\frac{n_a - n_b}{n_a + n_b})^2$$

where n_a and n_b represent the refractive index of medium-a and medium-b, respectively.

When there is only air-carbon black interface under dry condition,

$$R_{dry} = (\frac{1.00 - 1.60}{1.00 + 1.60})^2 = 5.33\ \%$$

The value of the reflectivity is calculated to be 5.33 %.

While there are both air-water and water-carbon black interfaces under wet condition,

$$R_{wet_1} = (\frac{1.00 - 1.33}{1.00 + 1.33})^2 = 2\ \%$$

$$R_{wet_2} = (\frac{1.33 - 1.60}{1.33 + 1.60})^2 = 0.85\ \%$$

$$R_{wet} \approx R_{wet_1} + R_{wet_2} = 2.85\ \%$$

Thus, the corresponding reflectivity is reduced to about 2.85 %. In the calculation, the contribution of water to the improvement of light absorption efficiency is excluded when water is transparent in visible spectra. Also, the calculation is based on the hypothesis that the incident light is normal to the interface and could not be affected by the reflected light.

Note S2

Influence of cross-sectional area and height on water injection rate

More experiments have already been carried out to reveal effects of the system volume on the evaporation performance. The volume of CBCS system is equal to cross-sectional area multiplied by height, so we explore effects of cross-sectional area and

height on the optimum water injection rate. The ability of water molecules to diffuse horizontally in CBCS is limited by surface tension. When cross-sectional area is enlarged, one water injection point cannot wet the whole cross-sectional area in time, which has a negative impact on evaporation performance. In our system, one water injection point can only quickly wet an area of about 50 cm2 in 120 seconds, thus multiple water injection points should be applied to eliminate the limitation of water-horizontal-diffusion ability on evaporation performance. When the height is fixed to 0.4 cm, the mass changes of CBCS with different cross-sectional areas were exhibited in Figure S13a and the calculated results of optimum water injection rate were shown in Figure S13c. It illustrated that the optimum water injection rate increases almost linearly with the increase of cross-sectional area.

Considering the situation that the water is injected from the bottom of CBCS system, the maximum wettable height (about 7 cm) of water in cellulose sponge is controlled by both capillary force and gravity, as exhibited in Figure S12. As the height of CBCS increases, more energy will be transferred to the bottom, thus results in a reduction of evaporation performance, which suggests a decrease of optimum injection rate. Therefore, the optimum injection rate decreases with the increase of height, as shown in Figure S13c which was calcualted from the mass changes of water in Figure S13a. In this work, a low height could supply a large wettability of cellulose sponge, but a too low height will cause a direct pass of incident light through CBCS, thus lead to a decrease of light absorption. Therefore, a proper height should be applied. In this work, a height of 0.4 cm was applied for improving evaporation performance.

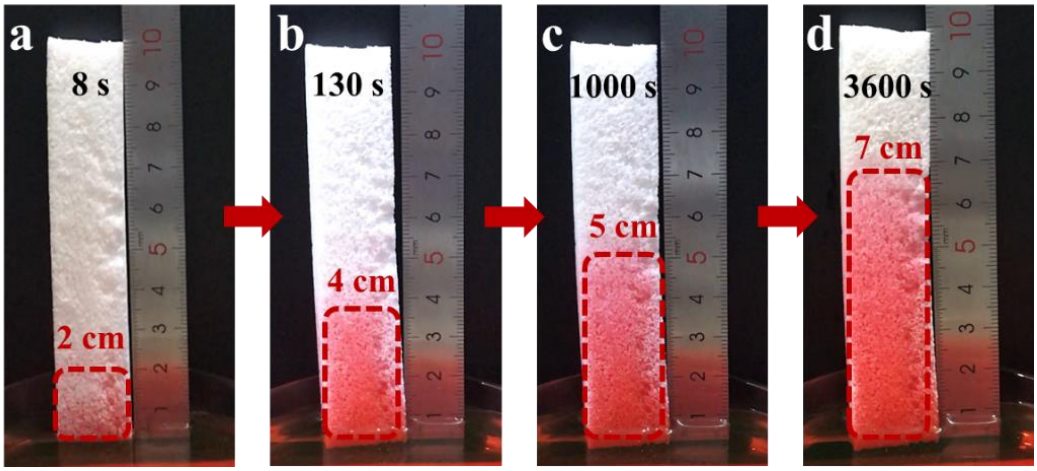

Figure S12. Wettable height of water in cellulose sponge with different contacting time.

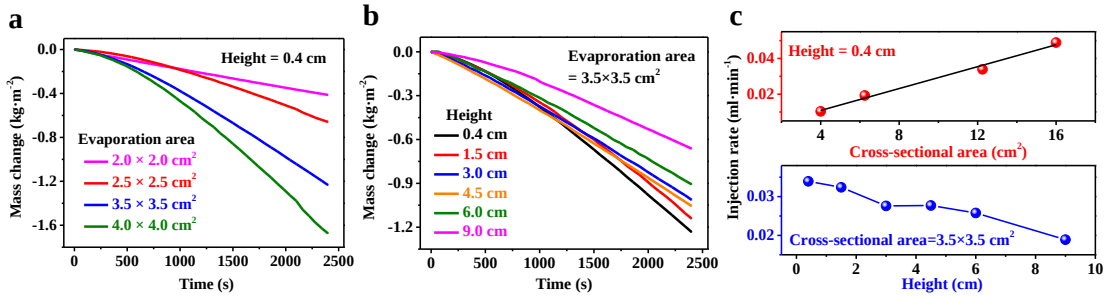

Figure S13. Mass change of CBCS with (a) different heights and (b) different evaporation areas; (c) optimum water injection rate of CBCS with different heights and evaporation areas.

Note S3

Energy loss analysis

The energy losses in CBCS with the concentration of carbon black particles of 20 g·L^{-1} [1] under one sun irradiation is calculated as an example. The energy consumption in the CBCS system can be divided into five main parts: (1) energy consumption by water

evaporation, (2) by the reflected solar light on surface, (3) by the conductive heat loss into EPE foam, (4) by the convective heat losses on the surface (5) by the radiative heat losses on the surface.

(1) Energy consumption by water evaporation.

Energy consumption through water evaporation equals to the evaporation efficiency, i. e. 91.5 % ($\eta_{eva} = 91.5\ \%$).

(2) Energy consumption by the reflected solar light on surface.

Considering the optical absorption of CBCS is about 97.5 %, the reflect heat loss should be about 2.5 % ($\eta_{ref} = 2.5\ \%$).

(3) Energy consumption by the conductive heat loss into EPE foam.

The heat conduction loss to bulk water can be calculated by the Fourier's law (i.e. $P_{cond} = k \cdot \frac{\Delta T}{L}$). k is the thermal conductivity of bulk water, and $\Delta T/L$ refers to the temperature gradient in the bulk water. However, the heat conduction loss to bulk water in present work is completely eliminated attributing to special water supply design. In this work, the heat conduction from CBCS to EPE foam can be simplified to one-dimensional steady state heat conduction, which can be calculated by $P_{cond_{EPE}} = \frac{k_{EPE}}{\delta}\Delta T$, where k_{EPE} is the thermal conductivity, δ is the thickness and ΔT is the temperature difference between inside and outside walls of the EPE foam. Thus, $P_{cond_{EPE}} = \frac{0.025}{0.0175} \times 5 \approx 7.14$ W·m^{-2}, $\eta_{cond_{EPE}} = 0.714\ \%$.

(4) Energy consumption by the convective heat losses on the surface.

The convection loss per unit area can be estimated by the Newton's law,

$$P_{conv} = h_c(T_2 - T_1)$$

where h_c stands the convective heat transfer coefficient, which can be calculated to be about 4.59 $W \cdot m^{-2} \cdot K^{-1}$ in this condition (more detailed calculation process can be referred to **Note S4** in Supporting information). It is noteworthy that the T_1 here refers to the average temperature of the air inside the concave groove (≈ 46 ℃) because of the special design of thermal-insulation concave groove. T_2 is the average temperature of absorber surface (about 50℃) under the steady state condition. Although T_1 and T_2 are affected by ambient temperature, the temperature difference between T_1 and T_2 is small due to the characteristics of thermal localization of CBCS system. Convection loss is calculated to be $P_{conv} = 4.585564 \times (50 - 46) \approx 18.34$ $W \cdot m^{-2}$, $\eta_{conv} = 1.834$ %.

(5) Energy consumption by the radiative heat losses on the surface.

The radiation loss per unit area can be calculated using the Stefan-Boltzmann law,

$$P_{rad} = \varepsilon\sigma(T_2^4 - T_1^4)$$

where ε is the emissivity of the CBCS sample assumed to be about 0.98 in this work, σ denotes the Stefan-Boltzmann constant, which is 5.67×10^{-8} $W \cdot m^{-2} \cdot K^{-4}$. Thus, P_{rad}= $0.98 \times 5.67 \times 10^{-8} \times (323.15^4 - 319.15^4) = 29.45$ $W \cdot m^{-2}$, $\eta_{conv} = 2.945$ %.

In summary, the total energy consumption of the five main parts is about 99.5 % (i.e. 91.5 % + 2.5 % +0.714 % + 1.834 % + 2.945 % ≈ 99.5 %), which follows the law of conservation of energy.

Note S4

Calculation of convective heat transfer coefficient (h_c):

In a natural convection problem, a dimensionless number, Rayleigh number (R_a), is critical in determination of h_c. Rayleigh number can be expressed as:

$$R_a = GrPr = \frac{g\beta(T_1 - T_2)l^3}{\upsilon^2}Pr$$

where Grashof number ($Gr = \frac{g\beta(T_1-T_2)l^3}{\upsilon^2}$) is a dimensionless number in heat transfer and hydrodynamics, which approximates the ratio of buoyancy to viscous force acting on a fluid. Prandtl number (Pr) is also a dimensionless number indicated the relationship between temperature boundary layer and flow boundary layer, which is defined as the ratio of momentum diffusivity to thermal diffusivity. g is the gravitational constant. β is coefficient of volume expansion, i.e. 1/T (K^{-1}). l is the characteristic length of the geometry (m). υ is the kinematics viscosity of the fluid (m^2/s). The sample in the experiment is a square with a side length of 3.5 cm.

The qualitative temperature $T_m = (T_1+T_2)/2 = 321$ K,

The relevant physical properties of air can be obtained at this temperature,

$B = 1/T_m = 3.12\times10^{-3}$ K^{-1},

$v = 1.78\times10^{-5}$ $m^2\cdot s^{-1}$ at 48 ℃,

$g = 9.8$ $m\cdot s^{-2}$,

$l = 3.5\times10^{-2}$ m,

$Pr = 0.698$ at 48 ℃,

Thus, $R_a = 8708$, $Gr = 1.25\times10^4$,

$Nu = 0.59 \times R_a^{0.25} = 5.7$,

$h_c = \frac{N_u \cdot k}{l} = 4.59\ \mathrm{W \cdot m^{-2} \cdot K^{-1}}$

It is worth noting that the humidity only has a negligible effect on kinematic viscosity and *Pr*. Also, the thermal conductivity of air at low temperature varies little with humidity.